A Nonlinear Concurrent Butterfly Equalizer

Kayol Soares MAYER, Jonathan Aguiar SOARES, Dalton Soares ARANTES

Dept. of Communications, University of Campinas – Unicamp, 400 Albert Einstein Ave., Campinas, Brazil

kayol@decom.fee.unicamp.br

Submitted November 4, 2020 / Accepted March 16, 2021

Abstract. *Optical communication systems operating with high data rates and dual-polarization are frequently disrupted by chromatic and polarization mode dispersions. Fixed filters usually mitigate chromatic dispersion; on the other hand, polarization mode dispersion (PMD), due to its stochastic behavior, is reduced by adaptive filters, such as channel equalizers. In this context, this article proposes a novel blind equalization architecture, based on the nonlinear modified concurrent equalizer (NMCE) expanded to a butterfly structure. The proposed nonlinear concurrent butterfly equalizer (NCBE) combines the reduced uncertainty and the sharper decision regions of the NMCE in both X and Y polarizations, resulting in improved performance. The NCBE is compared with the constant modulus algorithm (CMA), the modified CMA (MCMA), and the concurrent CMA-SDD (soft direct decision), all of them in butterfly architectures and with fractionally-spaced equalization. Results show that the proposed solution presents a reduced bit error rate (BER) and steady-state mean squared error (MSE) figures compared with the CMA, MCMA, and CMA-SDD equalizers the NCBE cross-shaped noise of the nonlinear equalizer output. Also, the NCBE can operate at higher values of PMD compared to the least mean square (LMS) equalizer without the necessity of delaying polarization X, Y, or both.*

Keywords

Data center interconnect, equalization architecture, blind equalizers, polarization mode dispersion

1. Introduction

In the last few years, with the development of big data analyses and the internet of things (IoT), technologies based on real-time processing have never been so important [1]. Real-time applications such as intelligent transportation systems and industry 4.0 need the computation of a large amount of data, which is usually processed in the cloud services [1], [2]. Currently, with this increasing demand, the data centers and the access networks, which play a key role in the cloud services, are requiring a high data rate transmission to meet the real-time processing specifications [3].

For intra data center interconnect (DCI) applications, optical transceivers can convey 400 Gb/s Ethernet data using parallel or multiple wavelength fibers [4]. Recently, single-carrier dual-polarization quadrature amplitude modulation (DP-QAM) has been proposed for DCI [5], [4]. In [4], the authors experimentally investigated the fiber transmission performance of single-carrier DP-16QAM and DP-64QAM aiming at 400 Gb/s and 600 Gb/s DCI applications for 40 km and beyond, over unamplified links.

In high data rate optical systems operating with dual-polarization (DP), chromatic dispersion and polarization mode dispersion (PMD) are two relevant sources of impairments [6]. As fiber chromatic dispersion is a time-invariant distortion, fixed filters are generally implemented to eliminate, or at least mitigate, this impairment [7], [8]. On the other hand, since PMD has a stochastic behavior, an adaptive filter (e.g., a channel equalizer) is necessary to compensate for this impairment while also tracking dynamic channel fluctuations [6, 8, 9].

Channel equalizers are commonly classified into three groups: supervised, semi-blind, and blind equalizers. Both supervised, and semi-blind equalizers depend upon a training sequence of known modulation symbols recurrently sent by the transmitter. For highly dynamic propagation scenarios, a longer training sequence is necessary to track the fast time-varying channel impulse response (CIR), which reduces the network transmission data rate. Since the training sequence conveys only specific information to train the equalizer, its use reduces the spectral efficiency of the system. In contrast, blind equalizers are only dependent on the statistical or geometrical characteristics of the received signal [10], [11].

The constant modulus algorithm (CMA) [12], [13] is one of the most cited blind equalizers for QAM modulation, as can be seen in several publications (e.g., [14–24]). Nevertheless, the CMA has a slow convergence rate and a significant residual mean squared error (MSE), in particular for high order modulation formats. Besides, it is not able to recover the phase of the received signal distorted by the channel impairments, which results in the rotation of the received symbols with respect to a reference constellation [18], [25]. In order to circumvent these CMA issues, modifications to the CMA cost function [25–27] and equalization architectures [17, 18, 28–30] have been proposed in

the last decades. For example, by splitting the CMA cost functions into real and imaginary components, the modified CMA (MCMA) [25] and its nonlinear version (NMCMA) [27] were proposed. Both MCMA and NMCMA can operate and recover the phase of the received symbols for low- and high-order QAM systems. Additionally, the NMCMA achieves better results than the MCMA due to the cohesion of the decision regions provided by the nonlinear sinusoidal transmittance, which increases the equalization robustness.

Otherwise, in [26] the authors proposed the so-called radius directed equalization (RDE), which, as opposed to the CMA, has its error function based on multi radii [31]. The RDE presents better performance in comparison to the CMA for low-order QAM (e.g., 16 and 64QAM); however, for high-order QAM (e.g., 256 and 1024QAM), as the radii number becomes large, the RDE has its convergence rate compromised [32].

On the other hand, by exploiting the complementarity properties of two well-known approaches, De Castro et al. [28] proposed an efficient method to circumvent the CMA issues, composed by the CMA and the direct decision (DD) [33], [34] equalizers operating in a concurrent architecture. Subsequently, based on this CMA-DD concurrent equalizer, Chen [29] replaced the DD equalizer by a soft direct decision (SDD) equalizer, thus achieving a faster convergence rate for the CMA-SDD when compared with the CMA-DD equalizer [29]. More recently, a novel concurrent architecture was proposed by Mayer et al., the NMCE equalizer [18]. The NMCE combines the sharper decision regions of the NMCMA with the reduced uncertainty of the SDD decisions, achieving improved performance even for operation in dynamic scenarios.

In such a context, this work proposes a new equalization architecture for optical communications with dual-polarization, based on the butterfly structure and the NMCE algorithm. In the proposed solution, the nonlinear concurrent architecture of the NMCE is expanded into a butterfly structure for both X and Y polarizations in a complete blind scheme. As a result, with the reduced uncertainty and the sharper decision regions of the NMCE, an improved performance is achieved even for operation in optical links with high dispersion between polarizations. The proposed nonlinear concurrent butterfly equalizer (NCBE) has been simulated with the Optisystem Design Tool for DP-256QAM under a DCI application (56 Gbaud per polarization) for a 40 km single-mode fiber link [4]. As a fixed filter generally eliminates the chromatic dispersion before the butterfly equalizer, simulations consider only PMD. Besides, phase noise has not been considered in the simulations, since phase correction is usually performed with pilot insertion or by the blind phase search (BPS) algorithm [35], apart from the butterfly equalization. Results show that the proposed NCBE achieves reduced figures of bit error rate (BER) and steady-state MSE when compared with CMA, MCMA, and CMA-SDD, all of them in butterfly architectures and with fractionally-spaced equalization (FSE) [36]. Also, the NCBE is able to operate at higher values of PMD in comparison with the least mean square (LMS) [37], dispensing with the time-consuming delay adjustments in polarizations X, Y, or both.

The remainder of this article is organized as follows. In Sec. 2, the butterfly equalization with FSE is presented in the context of coherent optical receivers. The main contribution of the present study is presented in Sec. 3: The proposed nonlinear concurrent butterfly equalizer for advanced optical receivers. In Sec. 4, the computational complexities of the LMS, CMA, MCMA, CMA-SDD, and NCBE algorithms are presented. Results are compared in terms of several values of PMD in Sec. 5. Conclusions are discussed in Sec. 6.

2. Butterfly Equalization for Fractionally Spaced Equalizers

In the literature, blind equalizers, when working with a sample rate (S_S) equal to the symbol rate (S_R), are generally convergent, provided the information source has a uniform distribution and the equalizer filter has a number of taps hypothetically larger than the infinite number of previous samples received from the channel [12]. In a practical application, however, the adopted number of equalizer taps should be finite but as large as necessary to achieve an acceptable convergence rate and steady-state MSE. If, however, the equalizer works with a higher sample rate $S_S = \Gamma S_R$, it is called a fractionally-spaced equalizer (FSE) [36], [38], where Γ is the upsampling factor. This oversampling procedure results in a shorter equalizer length while also avoiding the noise enhancement effect that occurs when the equalizer operates at symbol rate, and the channel transfer function has zeros on the unit circle of the z-plane [36]. In practice, the equalizer oversampling is most frequently chosen as $\Gamma = 2$ [39].

Four adaptive filters usually represent the butterfly structure for PMD equalization [6], [40], whose coefficients are updated by some supervised, semi-blind, or blind criterion. Regardless of the coefficients update technique, the butterfly equalizer handles both polarizations X and Y at the same time, as can be seen in Fig. 1, in which $k = 0, 1, \ldots, k \to \infty$ is the FSE discrete-time index for the sample rate $S_S = \Gamma S_R$.

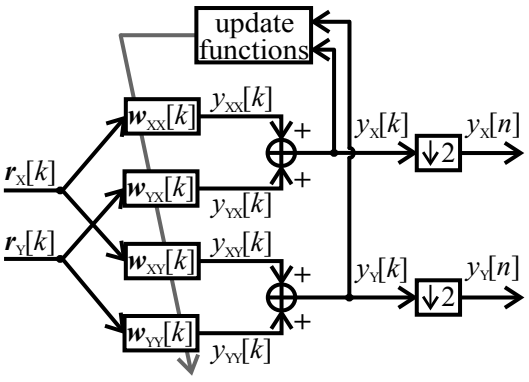

Fig. 1. Butterfly equalizer with FSE [20, 41, 42].

The upsampled inputs $r_X[k]$ and $r_Y[k]$, from polarizations X and Y, respectively, are convolved with the equalizer coefficient vectors $\boldsymbol{w}_{XX}[k]$, $\boldsymbol{w}_{YX}[k]$, $\boldsymbol{w}_{XY}[k]$, and $\boldsymbol{w}_{YY}[k]$ to produce the outputs $y_X[k]$ and $y_Y[k]$:

$$\begin{aligned} y_X[k] &= y_{XX}[k] + y_{YX}[k] \\ &= \boldsymbol{w}_{XX}[k]^T \boldsymbol{r}_X[k] + \boldsymbol{w}_{YX}[k]^T \boldsymbol{r}_Y[k], \end{aligned} \tag{1}$$

$$\begin{aligned} y_Y[k] &= y_{YY}[k] + y_{XY}[k] \\ &= \boldsymbol{w}_{YY}[k]^T \boldsymbol{r}_Y[k] + \boldsymbol{w}_{XY}[k]^T \boldsymbol{r}_X[k] \end{aligned} \tag{2}$$

where $[\cdot]^T$ denotes the vector transpose operator, $\boldsymbol{r}_X[k] = \begin{bmatrix} r_X[k] & r_X[k-1] & \cdots & r_X[k-L_{EQ}+1] \end{bmatrix}^T$, $\boldsymbol{r}_Y[k] = \begin{bmatrix} r_Y[k] & r_Y[k-1] & \cdots & r_Y[k-L_{EQ}+1] \end{bmatrix}^T$, $L_{EQ} \geq \Gamma L_{CH} - 1$ is the number of coefficients of the equalizer, and L_{CH} is the length of the channel impulse response. In addition, $\boldsymbol{w}_{XX}$, $\boldsymbol{w}_{XY}, \boldsymbol{w}_{YX}, \boldsymbol{w}_{YY} \in \mathbb{C}^{L_{EQ}\times 1}$.

The equalizer output signals $y_X[k]$ and $y_Y[k]$ are decimated by a factor of 2 to reproduce the output signals $y_X[n]$ and $y_Y[n]$, in which n is the discrete-time index, so that the sample rate $S_S = S_R$.

For supervised function adaptation, the LMS and the recursive least squares (RLS) [43] can be implemented to mitigate PMD. Nevertheless, as these algorithms rely on a reference training sequence at the receiver when the symbol sequence distortion is high, it is difficult to align the correct position of the training sequence concerning the symbol sequence. Another strategy is based on a hybrid scheme using both a supervised and a blind equalizer. In the beginning, a blind update function, such as the CMA, MCMA, or RDE, is used in a pre-equalization stage, improving the training sequence alignment. The blind update function is then switched to a supervised mode to improve the BER figure. However, for higher-order modulations, the CMA and MCMA performances deteriorate, and the RDE convergence is compromised [32].

3. Proposed Nonlinear Concurrent Butterfly Equalizer

Recently, as addressed in [18], the nonlinear modified concurrent equalizer (NMCE) was proposed for wireless communications of single-carrier systems. The NMCE is based on the soft concurrent approach (CMA-SDD) addressed in [44] and the NMCMA equalizer [27]. The NMCE combines the sharper decision regions of the NMCMA with the reduced uncertainty of the CMA-SDD, achieving improved performance [18]. Using as reference the NMCE, the nonlinear concurrent butterfly equalizer (NCBE), here proposed, in an FSE scheme with $\Gamma = 2$, as illustrated in Fig. 2. The superscripts {C} and {S} represent the NMCMA and the SDD linear components of the NCBE. Likewise, the superscript {NS} denotes the nonlinear part of the NCBE. Also, $f(\cdot)$ is the nonlinear transmittance presented in [18], which is given by:

$$f(b) = b + \alpha\left[\sin\left(\pi \mathrm{Re}\{b\}\right) + \mathrm{j}\sin\left(\pi \mathrm{Im}\{b\}\right)\right] \tag{3}$$

where b is any complex number and α is the nonlinear control parameter defined in the range of $[0, 1/\pi]$ [27]. For $\alpha = 0$, the NMCMA reduces to the MCMA equalizer [25]. $\mathrm{Re}\{\cdot\}$ and $\mathrm{Im}\{\cdot\}$ return the real and imaginary parts of their argument, respectively.

The NCBE output signals $y_X^{\{NS\}}[k]$ and $y_Y^{\{NS\}}[k]$ are given by

$$y_X^{\{NS\}}[k] = f\left(y_X^{\{CS\}}[k]\right), \tag{4}$$

$$y_Y^{\{NS\}}[k] = f\left(y_Y^{\{CS\}}[k]\right) \tag{5}$$

in which the linear output signals $y_X^{\{CS\}}[k]$ and $y_Y^{\{CS\}}[k]$ are

$$y_X^{\{CS\}}[k] = y_{XX}^{\{C\}}[k] + y_{XX}^{\{S\}}[k] + y_{YX}^{\{C\}}[k] + y_{YX}^{\{S\}}[k], \tag{6}$$

$$y_Y^{\{CS\}}[k] = y_{YY}^{\{C\}}[k] + y_{YY}^{\{S\}}[k] + y_{XY}^{\{C\}}[k] + y_{XY}^{\{S\}}[k]. \tag{7}$$

Two-by-two, the terms of the right-hand side of (6) and (7) can be represented as functions of the upsampled inputs $\boldsymbol{r}_X[k]$ and $\boldsymbol{r}_Y[k]$ and the coefficient vectors $\left(\boldsymbol{w}_{XX}^{\{C\}}, \boldsymbol{w}_{XY}^{\{C\}}, \boldsymbol{w}_{YX}^{\{C\}}, \boldsymbol{w}_{YY}^{\{C\}}, \boldsymbol{w}_{XX}^{\{S\}}, \boldsymbol{w}_{XY}^{\{S\}}, \boldsymbol{w}_{YX}^{\{S\}}, \boldsymbol{w}_{YY}^{\{S\}} \in \mathbb{C}^{L_{EQ}\times 1}\right)$ as:

$$y_{XX}^{\{C\}}[k] + y_{XX}^{\{S\}}[k] = \left(\boldsymbol{w}_{XX}^{\{C\}}[k] + \boldsymbol{w}_{XX}^{\{S\}}[k]\right)^T \boldsymbol{r}_X[k], \tag{8}$$

$$y_{YX}^{\{C\}}[k] + y_{YX}^{\{S\}}[k] = \left(\left(\boldsymbol{w}_{YX}^{\{C\}}[k] + \boldsymbol{w}_{YX}^{\{S\}}[k]\right)^T \boldsymbol{r}_Y[k], \tag{9}$$

$$y_{YY}^{\{C\}}[k] + y_{YY}^{\{S\}}[k] = \left(\left(\boldsymbol{w}_{YY}^{\{C\}}[k] + \boldsymbol{w}_{YY}^{\{S\}}[k]\right)^T \boldsymbol{r}_Y[k], \tag{10}$$

$$y_{XY}^{\{C\}}[k] + y_{XY}^{\{S\}}[k] = \left(\left(\boldsymbol{w}_{XY}^{\{C\}}[k] + \boldsymbol{w}_{XY}^{\{S\}}[k]\right)^T \boldsymbol{r}_X[k]. \tag{11}$$

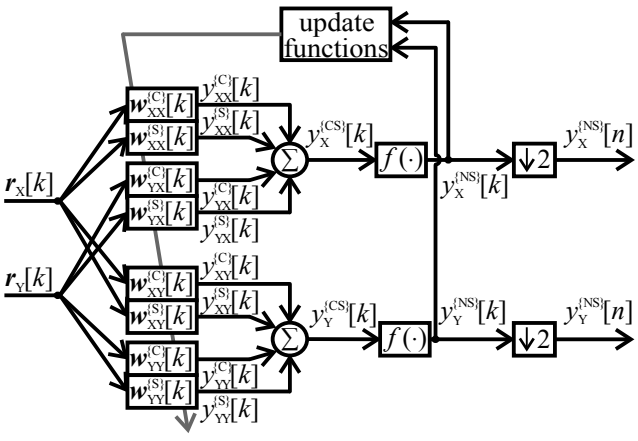

Fig. 2. Proposed nonlinear concurrent butterfly equalizer with FSE.

Based on [18], [27], and in the steepest descent algorithm, the update of the NMCMA coefficient vectors applied to the NCBE, are given as follows:

$$\boldsymbol{w}_{\mathrm{XX}}^{\{\mathrm{C}\}}[k+1] = \begin{cases} \boldsymbol{w}_{\mathrm{XX}}^{\{\mathrm{C}\}}[k] + \eta^{\{\mathrm{C}\}} e_{\mathrm{X}}^{\{\mathrm{C}\}}[k] \boldsymbol{r}_{\mathrm{X}}[k]^*, & \forall \text{ even } k, \\ \boldsymbol{w}_{\mathrm{XX}}^{\{\mathrm{C}\}}[k], & \forall \text{ odd } k, \end{cases} \tag{12}$$

$$\boldsymbol{w}_{\mathrm{YX}}^{\{\mathrm{C}\}}[k+1] = \begin{cases} \boldsymbol{w}_{\mathrm{YX}}^{\{\mathrm{C}\}}[k] + \eta^{\{\mathrm{C}\}} e_{\mathrm{X}}^{\{\mathrm{C}\}}[k] \boldsymbol{r}_{\mathrm{Y}}[k]^*, & \forall \text{ even } k, \\ \boldsymbol{w}_{\mathrm{YX}}^{\{\mathrm{C}\}}[k], & \forall \text{ odd } k, \end{cases} \tag{13}$$

$$\boldsymbol{w}_{\mathrm{XY}}^{\{\mathrm{C}\}}[k+1] = \begin{cases} \boldsymbol{w}_{\mathrm{XY}}^{\{\mathrm{C}\}}[k] + \eta^{\{\mathrm{C}\}} e_{\mathrm{Y}}^{\{\mathrm{C}\}}[k] \boldsymbol{r}_{\mathrm{X}}[k]^*, & \forall \text{ even } k, \\ \boldsymbol{w}_{\mathrm{XY}}^{\{\mathrm{C}\}}[k], & \forall \text{ odd } k, \end{cases} \tag{14}$$

$$\boldsymbol{w}_{\mathrm{YY}}^{\{\mathrm{C}\}}[k+1] = \begin{cases} \boldsymbol{w}_{\mathrm{YY}}^{\{\mathrm{C}\}}[k] + \eta^{\{\mathrm{C}\}} e_{\mathrm{Y}}^{\{\mathrm{C}\}}[k] \boldsymbol{r}_{\mathrm{Y}}[k]^*, & \forall \text{ even } k, \\ \boldsymbol{w}_{\mathrm{YY}}^{\{\mathrm{C}\}}[k], & \forall \text{ odd } k, \end{cases} \tag{15}$$

where $[\cdot]^*$ denotes the conjugate operator, $\eta^{\{\mathrm{C}\}}$ is the adaptive step of the coefficient vectors related to the NMCMA component of the NCBE, and $e_{\mathrm{X}}^{\{\mathrm{C}\}}[k] = \mathrm{Re}\{e_{\mathrm{X}}^{\{\mathrm{C}\}}[k]\} + \mathrm{j}\,\mathrm{Im}\{e_{\mathrm{X}}^{\{\mathrm{C}\}}[k]\}$ and $e_{\mathrm{Y}}^{\{\mathrm{C}\}}[k] = \mathrm{Re}\{e_{\mathrm{Y}}^{\{\mathrm{C}\}}[k]\} + \mathrm{j}\,\mathrm{Im}\{e_{\mathrm{Y}}^{\{\mathrm{C}\}}[k]\}$ are the error functions of the NMCMA component, with real and imaginary parts:

$$\mathrm{Re}\{e_{\mathrm{X}}^{\{\mathrm{C}\}}[k]\} = \mathrm{Re}\{y_{\mathrm{X}}^{\{\mathrm{NS}\}}[k]\}(\gamma_R - \mathrm{Re}\{y_{\mathrm{X}}^{\{\mathrm{NS}\}}[k]\}^2) \times \mathrm{Re}\{f'(y_{\mathrm{X}}^{\{\mathrm{CS}\}}[k])\}, \tag{16}$$

$$\mathrm{Im}\{e_{\mathrm{X}}^{\{\mathrm{C}\}}[k]\} = \mathrm{Im}\{y_{\mathrm{X}}^{\{\mathrm{NS}\}}[k]\}(\gamma_I - \mathrm{Im}\{y_{\mathrm{X}}^{\{\mathrm{NS}\}}[k]\}^2) \times \mathrm{Im}\{f'(y_{\mathrm{X}}^{\{\mathrm{CS}\}}[k])\}, \tag{17}$$

$$\mathrm{Re}\{e_{\mathrm{Y}}^{\{\mathrm{C}\}}[k]\} = \mathrm{Re}\{y_{\mathrm{Y}}^{\{\mathrm{NS}\}}[k]\}(\gamma_R - \mathrm{Re}\{y_{\mathrm{Y}}^{\{\mathrm{NS}\}}[k]\}^2) \times \mathrm{Re}\{f'(y_{\mathrm{Y}}^{\{\mathrm{CS}\}}[k])\}, \tag{18}$$

$$\mathrm{Im}\{e_{\mathrm{Y}}^{\{\mathrm{C}\}}[k]\} = \mathrm{Im}\{y_{\mathrm{Y}}^{\{\mathrm{NS}\}}[k]\}(\gamma_I - \mathrm{Im}\{y_{\mathrm{Y}}^{\{\mathrm{NS}\}}[k]\}^2) \times \mathrm{Im}\{f'(y_{\mathrm{Y}}^{\{\mathrm{CS}\}}[k])\} \tag{19}$$

in which γ_R and γ_I are the real and imaginary dispersion constants, respectively, as proposed in [25]. Also, $f'(\cdot)$ is the derivative of (3), which is given by:

$$f'(b) = [1 + \alpha\pi \cos(\pi \mathrm{Re}\{b\})] + \mathrm{j}[1 + \alpha\pi \cos(\pi \mathrm{Im}\{b\})]. \tag{20}$$

On the other hand, based on [18], [44], the update of the coefficient vectors relative to the SDD component of the NCBE, are given as:

$$\boldsymbol{w}_{\mathrm{XX}}^{\{\mathrm{S}\}}[k+1] = \begin{cases} \boldsymbol{w}_{\mathrm{XX}}^{\{\mathrm{S}\}}[k] + \eta^{\{\mathrm{S}\}} e_{\mathrm{X}}^{\{\mathrm{S}\}}[k] \boldsymbol{r}_{\mathrm{X}}[k]^*, & \forall \text{ even } k, \\ \boldsymbol{w}_{\mathrm{XX}}^{\{\mathrm{S}\}}[k], & \forall \text{ odd } k, \end{cases} \tag{21}$$

$$\boldsymbol{w}_{\mathrm{YX}}^{\{\mathrm{S}\}}[k+1] = \begin{cases} \boldsymbol{w}_{\mathrm{YX}}^{\{\mathrm{S}\}}[k] + \eta^{\{\mathrm{S}\}} e_{\mathrm{X}}^{\{\mathrm{S}\}}[k] \boldsymbol{r}_{\mathrm{Y}}[k]^*, & \forall \text{ even } k, \\ \boldsymbol{w}_{\mathrm{YX}}^{\{\mathrm{S}\}}[k], & \forall \text{ odd } k, \end{cases} \tag{22}$$

$$\boldsymbol{w}_{\mathrm{XY}}^{\{\mathrm{S}\}}[k+1] = \begin{cases} \boldsymbol{w}_{\mathrm{XY}}^{\{\mathrm{S}\}}[k] + \eta^{\{\mathrm{S}\}} e_{\mathrm{Y}}^{\{\mathrm{S}\}}[k] \boldsymbol{r}_{\mathrm{X}}[k]^*, & \forall \text{ even } k, \\ \boldsymbol{w}_{\mathrm{XY}}^{\{\mathrm{S}\}}[k], & \forall \text{ odd } k, \end{cases} \tag{23}$$

$$\boldsymbol{w}_{\mathrm{YY}}^{\{\mathrm{S}\}}[k+1] = \begin{cases} \boldsymbol{w}_{\mathrm{YY}}^{\{\mathrm{S}\}}[k] + \eta^{\{\mathrm{S}\}} e_{\mathrm{Y}}^{\{\mathrm{S}\}}[k] \boldsymbol{r}_{\mathrm{Y}}[k]^*, & \forall \text{ even } k, \\ \boldsymbol{w}_{\mathrm{YY}}^{\{\mathrm{S}\}}[k], & \forall \text{ odd } k, \end{cases} \tag{24}$$

where $\eta^{\{\mathrm{S}\}}$ is the adaptive step of the SDD components, and $e_{\mathrm{X}}^{\{\mathrm{S}\}}[k]$ and $e_{\mathrm{Y}}^{\{\mathrm{S}\}}[k]$ are the error functions, relative to the SDD component, which are given by

$$e_{\mathrm{X}}^{\{\mathrm{S}\}}[k] = \frac{1}{P_{\mathrm{X}}[k]} \sum_{p=2i-1}^{2i} \sum_{q=2l-1}^{2l} \exp\left(-\frac{|\xi_{\mathrm{X}}^{p,q}[k]|^2}{2\rho}\right) \xi_{\mathrm{X}}^{p,q}[k], \tag{25}$$

$$e_{\mathrm{Y}}^{\{\mathrm{S}\}}[k] = \frac{1}{P_{\mathrm{Y}}[k]} \sum_{p=2i-1}^{2i} \sum_{q=2l-1}^{2l} \exp\left(-\frac{|\xi_{\mathrm{Y}}^{p,q}[k]|^2}{2\rho}\right) \xi_{\mathrm{Y}}^{p,q}[k] \tag{26}$$

in which ρ is the SDD variance, $\xi_{\mathrm{X}}^{p,q}[k] = \mathcal{S}^{p,q} - y_{\mathrm{X}}^{\mathrm{NS}}[k]$ and $\xi_{\mathrm{Y}}^{p,q}[k] = \mathcal{S}^{p,q} - y_{\mathrm{Y}}^{\mathrm{NS}}[k]$ are the differences between the SDD reference symbol $\mathcal{S}^{p,q}$ [29] and the NCBE equalizer outputs, and $P_{\mathrm{X}}[k]$ and $P_{\mathrm{Y}}[k]$ are the *a posteriori* unnormalized probability density functions (PDF) of the SDD component, given by

$$P_{\mathrm{X}}[k] = \sum_{p=2i-1}^{2i} \sum_{q=2l-1}^{2l} \exp\left(-\frac{|\xi_{\mathrm{X}}^{p,q}[k]|^2}{2\rho}\right), \tag{27}$$

$$P_{\mathrm{Y}}[k] = \sum_{p=2i-1}^{2i} \sum_{q=2l-1}^{2l} \exp\left(-\frac{|\xi_{\mathrm{Y}}^{p,q}[k]|^2}{2\rho}\right). \tag{28}$$

The NCBE output signals $y_{\mathrm{X}}^{\mathrm{NS}}[k]$ and $y_{\mathrm{Y}}^{\mathrm{NS}}[k]$ are decimated by a factor of 2 to reproduce the outputs $y_{\mathrm{X}}^{\mathrm{NS}}[n]$ and $y_{\mathrm{Y}}^{\mathrm{NS}}[n]$, where n is the discrete-time index which corresponds to the sample rate $S_{\mathrm{S}} = S_{\mathrm{R}}$.

As in the NMCE equalizer, the coefficient vectors of the NCBE, relative to the NMCMA component, are initialized with a single spike scheme [18]. The single spike position, in the coefficient vectors, is dependent on the length of the channel impulse response. For symmetric channels (i.e.,

mixed-phase), a center spike is more appropriate. However, if the channel is asymmetric (i.e., minimum or non-minimum phase channels), the spike location should be moved towards the center of mass [45]. Also, in the context of butterfly equalization, as the NMCMA component of the NCBE is based on the CMA equalizer, the single spike should only be applied for the direct polarization coefficients (i.e., $\boldsymbol{w}_{\mathrm{XX}}^{\{\mathrm{C}\}}$ and $\boldsymbol{w}_{\mathrm{YY}}^{\{\mathrm{C}\}}$) [46]. This initialization scheme reduces the possibility of the equalizer output signals converging to only one of the two polarizations.

In optical channels with PMD, the differential group delay (DGD) follows a Maxwellian distribution [47]. Thus, taking into account the major part of the delays between both polarizations, a channel with PMD can be considered a mixed-phase channel centered at the mean DGD ($\bar{\tau}$). Furthermore, the mean DGD can be discretely represented in terms of the number of upsampled symbols as:

$$\delta = \lceil \bar{\tau} \Gamma S_{\mathrm{R}} \rceil \tag{29}$$

where $\lceil \cdot \rceil$ is the operator that returns the smallest integer greater than its argument. In view of (29), the single spike position in the direct polarization coefficients can be defined as: if $\delta = 1$, then the single spike is applied at the first coefficient since the equalizer approximates the PMD as a minimum phase channel; on the other hand, if $1 < \delta < L_{\mathrm{EQ}}$, then the single spike is applied at the center tap of the coefficients (mixed-phase representation); finally, if $\delta \geq L_{\mathrm{EQ}}$, then the single spike is applied at the last coefficient (non-minimum phase representation). Note that, if $\delta > L_{\mathrm{EQ}}$, the mean channel dispersion is greater than the number of coefficients of the equalizer.

4. Computational Complexities

Table 1 presents the computational complexities of the LMS, CMA, MCMA, CMA-SDD, and NCBE butterfly equalizers with FSE, recalling that L_{EQ} is the number of coefficients of the equalizer. Since $\sin(\cdot)$ and $\exp(\cdot)$ functions can be easily implemented in hardware by lookup tables, multiplication is the most costly operation. One may note that the proposed NCBE presents only a slightly higher complexity when compared with the CMA-SDD complexity.

Equalizers	×	+	exp(·)	sin(·)
LMS	$32L_{\mathrm{EQ}} + 4$	$32L_{\mathrm{EQ}}$	0	0
CMA	$32L_{\mathrm{EQ}} + 10$	$32L_{\mathrm{EQ}}$	0	0
MCMA	$32L_{\mathrm{EQ}} + 12$	$32L_{\mathrm{EQ}}$	0	0
CMA-SDD	$48L_{\mathrm{EQ}} + 46$	$56L_{\mathrm{EQ}} + 42$	8	0
NCBE	$48L_{\mathrm{EQ}} + 78$	$56L_{\mathrm{EQ}} + 50$	8	8

Tab. 1. Computational complexities. The operators ×, +, exp(·), and sin(·) are denoted to the number of multiplications, additions, exponential, and sinusoidal functions, respectively.

5. Simulation Results

The butterfly equalizers for the LMS, CMA, MCMA, CMA-SDD, and the proposed NCBE, have been simulated with the Optisystem Design Tool for DP-256QAM under a DCI application (56 Gbaud per polarization) for a 40 km single-mode fiber link [4], [49].

In the Optisystem platform, at the transmitter side, the stream of bits is generated by a pseudo-random generator with uniform distribution at a rate of 896 Gb/s. This stream of bits is then split into polarizations X and Y. These two bitstreams are then separately modulated into 256QAM constellations with Gray code at a rate of 56 Gbaud per polarization. Subsequently, the symbol streams are upsampled with 16 samples per symbol and filtered by a root-raised cosine (RRC) filter with a roll-off factor of 0.2 [4]. Next, the two polarizations are converted, combined and transformed from the electrical to the optical domain by cascading a laser source (193.4 THz) with Mach-Zehnder modulators (MZM) and a polarization beam combiner (PBC) [4].

The optical fiber link simulated in the Optisystem platform considers an unamplified single-mode link with $l = 40$ km [4]. Also, as a fixed filter generally eliminates the chromatic dispersion before the butterfly equalizer [7], [8], simulations consider only PMD, in varying steps from 1 ps/km to 10 ps/km. Besides, phase noise has not been simulated since phase correction is usually performed apart from the butterfly equalization.

At the receiver, the optical signal is first demodulated by using a 90° heterodyne coherent detector. The resulting electrical signal is initially processed by an analog-to-digital converter (ADC), operating at 16 samples per symbol, then processed by the RRC filter, and, finally, downsampled to deliver two samples per symbol for the posterior FSE equalization [4].

In order to compare the NCBE with the LMS, CMA, MCMA, and CMA-SDD algorithms, 10 runs of simulation with 2^{19} symbols per polarization were performed using the Optisystem platform. For the BER computation, only the last 2^{17} symbols of each polarization was considered, and the results were averaged over ten runs of simulation for each value of DGD. Also, a soft-decision forward error correction (SD-FEC) BER threshold of 4.2×10^{-2} [4], [48], is used to compare the equalizer's penalties. The convergence time is assessed from 1 ps/km to 8 ps/km of relative dispersion. Also, the MSE and scatter plots for the constellations of the X and Y polarizations, for the relative dispersion of 8 ps/km, are presented to address the NCBE nonlinear cross effect.

The same operating conditions have been applied to the CMA, MCMA, CMA-SDD, and NCBE equalizers, but a hypothetical case has been considered in which the LMS was trained for all received symbols. The number of coefficients of each equalizer was set to $L_{\mathrm{EQ}} = 21$ [4], [49].

In light of the previous considerations, the initialization schemes have been chosen as follows:

- The initialization of the filter coefficients of the CMA, MCMA, CMA of the CMA-SDD, and the NMCMA component of the NCBE, follows the single spike method, but only applied to the direct polarization coefficients [46];
- The coefficient vectors of the LMS and the SDD components of the CMA-SDD and the NCBE start with all elements equal to zero;
- The SDD variances of the CMA-SDD and the NCBE are set to $\rho = 0.4$;
- The adaptive steps are: LMS is 1×10^{-6}; CMA is 9×10^{-9}; MCMA is 9×10^{-9}; the CMA-SDD is 9×10^{-9} for the CMA and 2×10^{-5} for the SDD; and the NCBE is 9×10^{-9} for the NMCMA and 2×10^{-5} for the SDD;
- The nonlinear control parameter for the NMCMA component of the NCBE was set to $\alpha = 0.30$;
- The dispersion constants of the MCMA and the NMCMA component of the NCBE are $\gamma_R = \gamma_I = 152.2$, and of the CMA and the CMA component of the CMA-SDD is $\gamma = 237.2$.

Figure 3 presents the PMD penalty curves of the discussed equalizers relative to the back-to-back BER. Although trained for the whole sequence of received symbols, when the relative dispersion $(\bar{\tau}/l)$ is greater than 5 ps/km, the LMS does not converge. Using (29), this dispersion is equivalent to $\delta = 23$ symbols, which exceeds the number of coefficients of the LMS equalizer. To circumvent this issue, it is necessary to increase the number of coefficients of the LMS or to delay one of the two polarizations. Thus, in a practical approach, in order to align the training sequence for the proper LMS adaptation, it would be necessary to test a set of different delays for both polarizations to reach the convergence of the LMS algorithm, which is a big issue, especially for low-power scenarios [50]. On the other hand, via the single spike method, the CMA-based equalizers (i.e., CMA, MCMA, CMA-SDD, and NCBE) are able to operate up to a relative dispersion of 9 ps/km, which is equivalent to $\delta = 41$ symbols. Thus, regarding only the CMA-based equalizers, the NCBE presents better penalty gains around 0.25 dB, 1.0 dB, and 3.1 dB in comparison with the CMA-SDD, MCMA, and CMA equalizers, respectively.

Figures 4 and 5 present the BER versus OSNR results for the CMA, MCMA, CMA-SDD, and NCBE equalizers. The BER×OSNR simulations disregard the LMS equalizer because of its convergence issue, which could demand a prohibitively high computational complexity in a practical scenario. In Fig. 4, for the working region around and below BER $\approx 1 \times 10^{-2}$, the NCBE presents a penalty of only 1.0 dB in comparison with the back-to-back system, whereas the CMA, MCMA, and CMA-SDD have penalties around 10.0 dB, 5.0 dB, and 1.3 dB, respectively. When the relative dispersion becomes more prominent, as in Fig. 5, the equalizers' performance is worsened. However, considering once again the region for BER $\leq 1 \times 10^{-2}$, the NCBE has its penalty increased to 2.0 dB, whereas the CMA, MCMA, and CMA-SDD have their penalties increased to approximately 15.0 dB, 9.0 dB, and 2.2 dB, respectively.

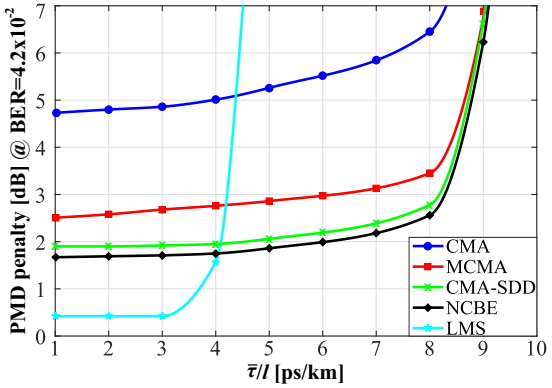

Fig. 3. DP-256QAM simulation results for the LMS, CMA, MCMA, CMA-SDD, and NCBE equalizers, showing the PMD penalty relative to the back-to-back BER with FEC threshold of 4.2×10^{-2} [4], [48].

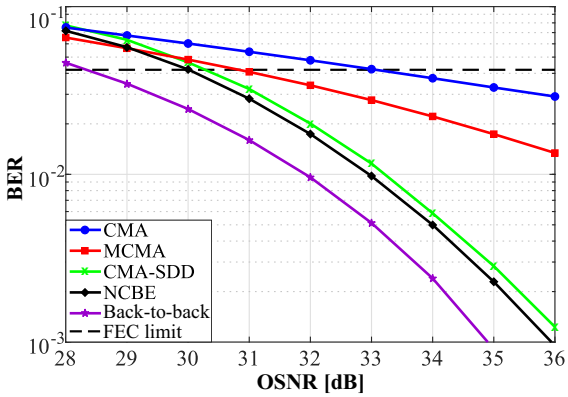

Fig. 4. DP-256QAM BER simulation results for the CMA, MCMA, CMA-SDD, and NCBE equalizers for $\bar{\tau}/l$ = 1 ps/km and for a reference bandwidth of 12.5 GHz to measure the OSNR [50].

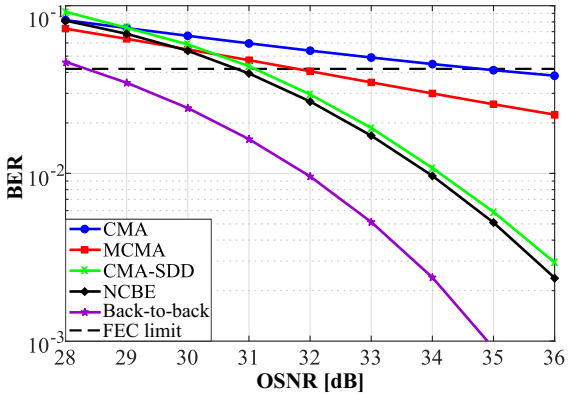

Fig. 5. DP-256QAM BER simulation results for the CMA, MCMA, CMA-SDD, and NCBE equalizers, for $\bar{\tau}/l$ = 8 ps/km and a reference bandwidth of 12.5 GHz to measure the OSNR [50].

Figure 6 presents the convergence rates for the CMA, MCMA, CMA-SDD, and NCBE equalizers for 36 dB of OSNR. The simulated blind equalizers have a fast convergence rate, even for the worst case of $\bar{\tau}/l = 8$ ps/km, for which the equalizers' convergences are achieved before 5×10^5 symbols. However, for higher values of PMD, the concurrent architectures (i.e., CMA-SDD and NCBE) are able to reach convergence twice as faster as the CMA and MCMA equalizers.

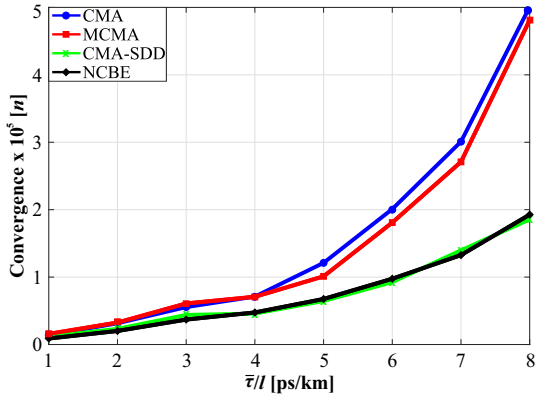

Fig. 6. DP-256QAM convergence results for the CMA, MCMA, CMA-SDD, and NCBE equalizers, for OSNR = 36 dB.

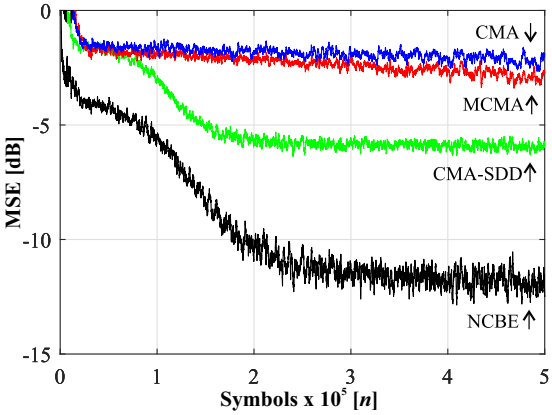

Fig. 7. DP-256QAM X polarization MSE results for the CMA, MCMA, CMA-SDD, and NCBE equalizers, for OSNR = 36 dB and $\bar{\tau}/l = 8$ ps/km.

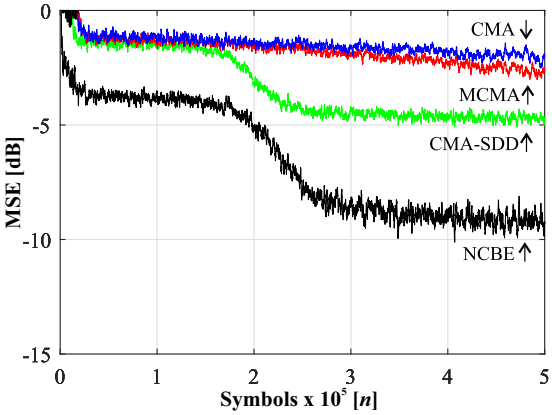

Fig. 8. DP-256QAM Y polarization MSE results for the CMA, MCMA, CMA-SDD, and NCBE equalizers, for OSNR = 36 dB and $\bar{\tau}/l = 8$ ps/km.

Figures 7, 8, and 9 present the evolution of the MSE during equalization and the scatter plots for the constellations of the CMA, MCMA, CMA-SDD, and NCBE equalizers, for 36 dB of OSNR and $\bar{\tau}/l = 8$ ps/km. In Figs. 7 and 8, where the CMA and the MCMA have a significant residual steady-state MSE, of approximately −2.5 dB, the CMA-SDD and the NCBE achieve −5.0 dB and −10.0 dB of residual MSE, respectively. It is also evident that the NCBE shows an impressive residual steady-state MSE gain of 5.0 dB when

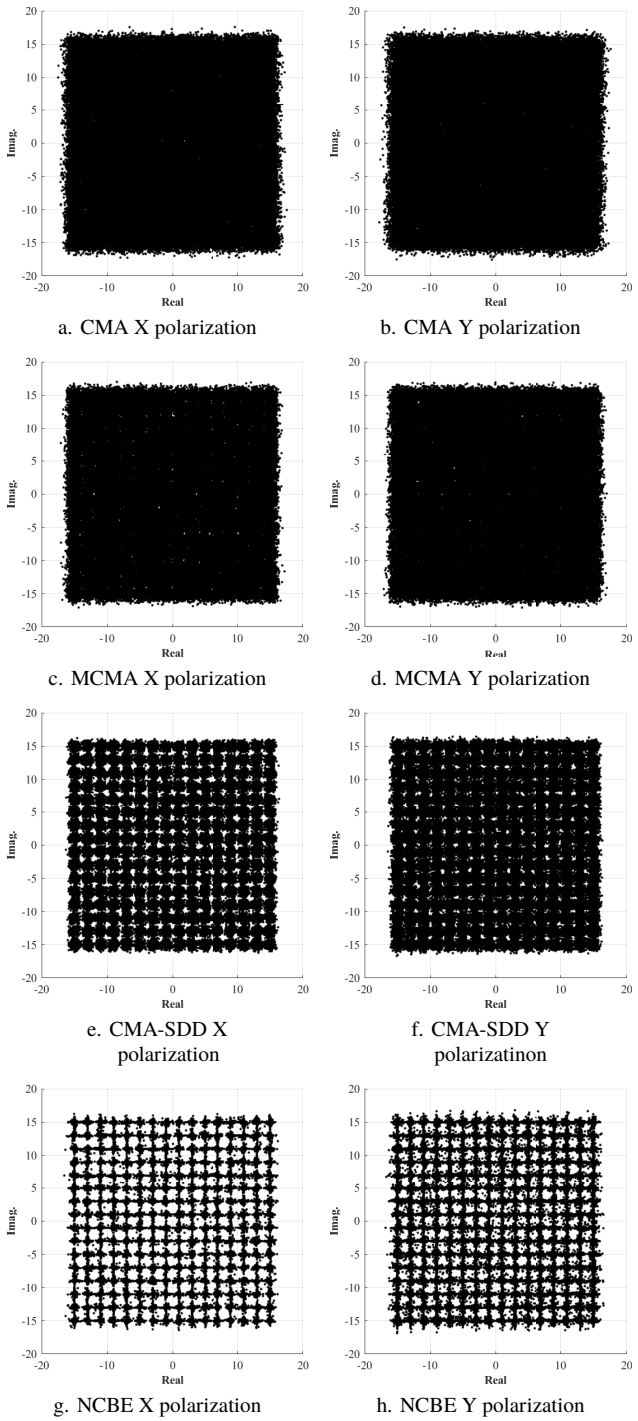

a. CMA X polarization
b. CMA Y polarization
c. MCMA X polarization
d. MCMA Y polarization
e. CMA-SDD X polarization
f. CMA-SDD Y polarizatinon
g. NCBE X polarization
h. NCBE Y polarization

Fig. 9. DP-256QAM scatter plot results for OSNR= 36 dB and $\bar{\tau}/l = 8$ ps/km.

compared with the CMA-SDD. However, this significant gain is not reflected in the BER figures shown in Fig. 5, in which the BER gain of the NCBE is 0.3 dB when compared with the CMA-SDD. This is a consequence of the nonlinear cross effect manifested in the residual noise of the NCBE algorithm illustrated in Figs. 9g and 9h. Differently from the CMA, MCMA, and CMA-SDD scatter plots shown in Figs. 9a–f, in which the output symbols appear with Gaussian distributions around the reference symbols, the NCBE output symbols are distributed in a conspicuous cross pattern. Due to the NCBE nonlinear transmittance, the output symbols are compressed in the real and imaginary axes, increasing the cohesion of the decision regions. The collapse of the cross-shaped noise variances along the diagonal axes of the reference symbols, relative to the variances along the real and imaginary axes, may explain why the residual MSE results are significantly more optimistic than the BER figures obtained for the NCBE equalizer.

It is also important to emphasize the fast convergence rates of the CMA-SDD and NCBE equalizers since a shorter preamble may be needed in practical system implementation. This leads to lower bit-rate overhead and faster operation during system startup or synch recovery. Since a faster convergence rate implies lower adaptation inertia, the NCBE equalizer may also be effective under dynamic channel perturbations.

As future work, it is interesting to investigate whether the peculiar cross-shaped noise at the output of the NCBE equalizer could lead to additional gains in terms of system capacity. In other words, the question is whether the minimal relative value of the steady-state MSE of the NCBE would result in additional gains with the use of some specific forward error correction (FEC) code matched to the cross-shaped noise. Strong candidates would probably include the family of unequal error protection codes, but this needs further investigation.

6. Conclusion

This work presents a novel blind equalization scheme for high-order and high baud-rate DP-QAM optical systems. The proposed nonlinear concurrent butterfly equalizer (NCBE) combines the nonlinear concurrent architecture of the NMCE with the 2×2 structure of the butterfly equalizer, resulting in a modified butterfly equalizer. This concurrent architecture can recover the phases of both X and Y polarizations and operate at higher-values of PMD when compared even with the LMS butterfly equalizer at the same level of computational complexity.

The performance of the proposed approach was compared with those of the LMS, CMA, MCMA, and CMA-SDD butterfly equalizers under several values of PMD. All simulations were performed with the Optisystem Design Tool, focusing on a 40 km single-mode fiber DCI application with DP-256QAM and 56 Gbaud per polarization.

The proposed butterfly architecture proved to be robust under several PMD dispersion values, achieving lower penalties and overall better performances when compared with the CMA, MCMA, and CMA-SDD butterfly equalizers. For $\bar{\tau}/l = 1$ ps/km, the NCBE presented a BER penalty of only 1.0 dB with respect to the back-to-back configuration, whereas the CMA, MCMA, and CMA-SDD, presented penalties around 10.0 dB, 5.0 dB, and 1.3 dB, respectively. Under the higher relative dispersion of $\bar{\tau}/l = 8$ ps/km, the NCBE has its power penalty increased to 2.0 dB, whereas the CMA, MCMA, and CMA-SDD have their penalties increased to approximately 15.0 dB, 9.0 dB, and 2.2 dB, respectively. Also, while the LMS is not able to operate for relative dispersions greater than its filter length (without increasing the computational complexity), the NCBE is able to function up to a relative dispersion twice as large as its filter length.

Acknowledgments

Kayol S. Mayer is supported in part by the Coordenação de Aperfeiçoamento de Pessoal de Nível Superior – Brasil (CAPES) – Finance Code 001.

Jonathan A. Soares is supported in part by the National Council for Scientific and Technological Development – Brasil (CNPq) – Grant number 132545/2019-5.

The authors wish to acknowledge the Optiwave Systems Inc. for their invaluable support with an academic license of the Optisystem Design Tool.

References

[1] KNIEPS, G. Internet of Things, big data and the economics of networked vehicles. *Telecommunications Policy*, 2019, vol. 43, no. 2, p. 171–181. DOI: 10.1016/j.telpol.2018.09.002

[2] RAPTIS, T. P., PASSARELLA, A., CONTI, M. Data management in industry 4.0: State of the art and open challenges. *IEEE Access*, 2019, vol. 7, p. 97052–97093. DOI: 10.1109/ACCESS.2019.2929296

[3] ZOU, D., LI, Z., SUN, Y., et al. Computational complexity comparison of single-carrier DMT and conventional DMT in data center interconnect. *Optics Express*, 2019, vol. 27, no. 12, p. 17007–17016. DOI: 10.1364/OE.27.017007

[4] YUE, Y., WANG, Q., ANDERSON, J. Experimental investigation of 400 Gb/s data center interconnect using unamplified high-baud-rate and high-order QAM single-carrier signal. *Applied Sciences*, 2019, vol. 9, no. 12, p. 1–9. DOI: 10.3390/app9122455

[5] SONE, Y., NISHIZAWA, H., YAMAMOTO, S., et al. Systems and technologies for high-speed inter-office/datacenter interface. In *Proceedings of SPIE Photonics West*. San Francisco (United States), 2017, p. 73–80. DOI: 10.1117/12.2256553

[6] IP, E., KAHN, J. M. Digital equalization of chromatic dispersion and polarization mode dispersion. *Journal of Lightwave Technology*, 2007, vol. 25, no. 8, p. 2033–2043. DOI: 10.1109/JLT.2007.900889

[7] SAVORY, S. J. Digital coherent optical receivers: Algorithms and subsystems. *IEEE Journal of Selected Topics in Quantum Electronics*, 2010, vol. 16, no. 5, p. 1164–1179. DOI: 10.1109/JSTQE.2010.2044751

[8] MALEKIHA, M., TSELNIKER, I., PLANT, D. V. Chromatic dispersion mitigation in long-haul fiber-optic communication networks by sub-band partitioning. *Optics Express*, 2015, vol. 23, no. 25, p. 32654–32663. DOI: 10.1364/OE.23.032654

[9] YAN, L., HAUER, M. C., SHI, Y., et al. Polarization-mode-dispersion emulator using variable differential-group-delay (DGD) elements and its use for experimental importance sampling. *Journal of Lightwave Technology*, 2004, vol. 22, no. 4, p. 1051–1058. DOI: 10.1109/JLT.2004.825327

[10] CHI, C. Y., CHEN, C. Y., CHEN, C. H., et al. Batch processing algorithms for blind equalization using higher-order statistics. *IEEE Signal Processing Magazine*, 2003, vol. 20, no. 1, p. 25–49. DOI: 10.1109/MSP.2003.1166627

[11] GU, M., TONG, L. Geometrical characterizations of constant modulus receivers. *IEEE Transactions on Signal Processing*, 1999, vol. 47, no. 10, p. 2745–2756. DOI: 10.1109/78.790656

[12] GODARD, D. Self-recovering equalization and carrier tracking in two-dimensional data communication systems. *IEEE Transactions on Communications*, 1980, vol. 28, no. 11, p. 1867–1875. DOI: 10.1109/TCOM.1980.1094608

[13] LIU, N., JU, C., LI, C. Parallel implementation of hardware-efficient adaptive equalization for coherent PON systems. *Optical and Quantum Electronics*, 2021, vol. 53, no. 20, p. 1–16. DOI: 10.1007/s11082-020-02681-2

[14] FARUK, M. S. Blind equalization and carrier-phase recovery based on modified constant-modulus algorithm in PDM-QPSK coherent optical receivers. *Optical and Quantum Electronics*, 2015, vol. 48, no. 3, p. 1–9. DOI: 10.1007/s11082-015-0270-7

[15] MATSUDA, K., MATSUMOTO, R., SUZUKI, N. Hardware-efficient adaptive equalization and carrier phase recovery for 100-Gb/s/λ-based coherent WDM-PON systems. *Journal of Lightwave Technology*, 2018, vol. 36, no. 8, p. 1492–1497. DOI: 10.1109/JLT.2017.2784804

[16] JIANG, W.-J., KUZMIN, K. G., WAY, W. I. Effect of low oversampling rate on a 64Gbaud/DP-16QAM 100-km optical link. *IEEE Photonics Technology Letters*, 2018, vol. 30, no. 19, p. 1671–1674. DOI: 10.1109/LPT.2018.2864639

[17] MAYER, K. S., DE OLIVEIRA, M. S., MÜLLER, C., et al. Blind fuzzy adaptation step control for a concurrent neural network equalizer. *Wireless Communications and Mobile Computing*, 2019, vol. 2019, p. 1–11. DOI: 10.1155/2019/9082362

[18] MAYER, K. S., MÜLLER, C., DE CASTRO, M. C. F., et al. Nonlinear modified concurrent equalizer. *Journal of Communication and Information Systems*, 2019, vol. 34, no. 1, p. 200–205. DOI: 10.14209/jcis.2019.21

[19] MAYER, K. S., MÜLLER, C., DE CASTRO, F. C. C., et al. A new CPFSK demodulation approach for software defined radio. *Journal of Circuits, Systems, and Computers*, 2019, vol. 28, no. 14, p. 1–14. DOI: 10.1142/S0218126619502438

[20] MAYER, K. S., MOREIRA, V. R., SOARES, J. A., et al. High data-rates and high-order DP-QAM optical links can be efficiently implemented with concurrent equalization. In *Proceedings of Photonics North (PN)*. Niagara Falls (Canada), 2020, p. 1. DOI: 10.1109/PN50013.2020.9167008

[21] AHMED, S., KHAN, Y. A review on training and blind equalization algorithms for wireless communications. *Wireless Personal Communications*, 2019, vol. 108, no. 3, p. 1759–1783. DOI: 10.1007/s11277-019-06495-8

[22] TANIZAWA, K., FUTAMI, F. Digital coherent 20-Gbit/s DP-PSK Y-00 quantum stream cipher transmission over 800-km SSMF. In *Proceedings of Optical Fiber Communications Conference and Exposition (OFC)*. San Diego (United States), 2019, p. 1–3. DOI: 10.1364/OFC.2019.Th1J.7

[23] LU, J., WU, Q., JIANG, H. et al. Efficient timing/frequency synchronization based on sparse fast Fourier transform. *Journal of Lightwave Technology*, 2019, vol. 37, no. 20, p. 5299–5308. DOI: 10.1109/JLT.2019.2932075

[24] JIANG, L., YAN, L., YI, A, et al. Blind optical modulation format identification assisted by signal intensity fluctuation for autonomous digital coherent receivers. *Optics Express*, 2020, vol. 28, no. 1, p. 302–313. DOI: 10.1364/OE.372406

[25] OH, K. N., CHIN, Y. O. Modified constant modulus algorithm: Blind equalization and carrier phase recovery algorithm. In *Proceedings IEEE International Conference on Communications (ICC)*. Seattle (USA), 1995, p. 498–502. DOI: 10.1109/ICC.1995.525219

[26] READY, M. J., GOOCH, R. P. Blind equalization based on radius directed adaptation. In *Proceedings of International Conference on Acoustics, Speech, and Signal Processing (ICASSP)*. Albuquerque (USA), 1990, p. 1699–1702. DOI: 10.1109/ICASSP.1990.115806

[27] WANG, D. A nonlinear modified constant modulus algorithm for blind equalization. In *Canadian Conference on Electrical and Computer Engineering (CCECE)*. Calgary (Canada), 2010, p. 1–4. DOI: 10.1109/CCECE.2010.5575240

[28] DE CASTRO, F. C. C., DE CASTRO, M. C. F., ARANTES, D. S. Concurrent blind deconvolution for channel equalization. In *IEEE International Conference on Communications (ICC)*. Helsinki (Finland), 2001, p. 366–371. DOI: 10.1109/ICC.2001.936964

[29] CHEN, S. Low complexity concurrent constant modulus algorithm and soft decision directed scheme for blind equalisation. *IEE Proceedings - Vision, Image, and Signal Processing*, 2003, vol. 150, no. 5, p. 312–320. DOI: 10.1049/ip-vis:20030619

[30] SILVA, M. T. M., ARENAS-GARCIA, J. A soft-switching blind equalization scheme via convex combination of adaptive filters. *IEEE Transactions on Signal Processing*, 2013, vol. 61, no. 5, p. 1171–1182. DOI: 10.1109/TSP.2012.2236835

[31] KAMRAN, R., NAMBATH, N., MANIKANDAN, S., et al. Demonstration of a low-power, local-oscillator-less, and DSP-free coherent receiver for data center interconnects. *Applied Optics*, 2020, vol. 59, no. 7, p. 2031–2041. DOI: 10.1364/AO.383185

[32] GUIOMAR, F. P., AMADO, S. B., CARENA, A., et al. Fully blind linear and nonlinear equalization for 100G PM-64QAM optical system. *Journal of Lightwave Technology*, 2015, vol. 33, no. 7, p. 1265–1274. DOI: 10.1109/JLT.2014.2386653

[33] MACCHI, O., EWEDA, E. Convergence analysis of self-adaptive equalizers. *IEEE Transactions on Information Theory*, 1984, vol. 30, no. 2, p. 161–176. DOI: 10.1109/TIT.1984.1056896

[34] KONG, M., WANG, K., DING, J., et al. 640-Gbps/carrier WDM transmission over 6,400 km based on PS-16QAM at 106 Gbaud employing advanced DSP. *Journal of Lightwave Technology*, 2021, vol. 39, no. 1, p. 55–63. DOI: 10.1109/JLT.2020.3024771

[35] PFAU, T., HOFFMANN, S., NOE, R. Hardware-efficient coherent digital receiver concept with feedforward carrier recovery for M-QAM constellations. *Journal of Lightwave Technology*, 2009, vol. 27, no. 8, p. 989–999. DOI: 10.1109/JLT.2008.2010511

[36] GITLIN, R. D., WEINSTEIN, S. B. Fractionally-spaced equalization: An improved digital transversal equalizer. *Bell System Technical Journal*, 1981, vol. 60, no. 2, p. 275–296. DOI: 10.1002/j.1538-7305.1981.tb00240.x

[37] MAYER, K. S., SOARES, J. A., ARANTES, D. S. Complex MIMO RBF neural networks for transmitter beamforming over nonlinear channels. *Sensors*, 2020, vol. 20, no. 2, p. 1–15. DOI: 10.3390/s20020378

[38] JOHNSON, R., SCHNITER, P., ENDRES, T., et al. Blind equalization using the constant modulus criterion: a review. *Proceedings of the IEEE*, 1998, vol. 86, no. 10, p. 1927–1950. DOI: 10.1109/5.720246

[39] FAIG, H., SADOT, D., GANTZ, L., et al. An efficient stabilization process for analog fractionally spaced equalizers. *IEEE Photonics Technology Letters*, 2019, vol. 31, no. 9, p. 665–668. DOI: 10.1109/LPT.2019.2903275

[40] ZHANG, R., KUZMIN, K., JIAN, W.-J., et al. Impact of laser flicker noise and linewidth on 64 to 96 Gbaud/DP-nQAM metro coherent optical links. *Optics Letters*, 2020, vol. 45, no. 5, p. 1220–1223. DOI: 10.1364/OL.386267

[41] ZENG, T., HE, Z., MENG, L., et al. The real time implementation of a simplified 2-section equalizer with supernal SOP tracking capability. In *Proceedings of Optical Fiber Communications Conference and Exposition (OFC)*. San Diego (United States), 2020, p. 1–3. DOI: 10.1364/OFC.2020.M2J.7

[42] NAMBATH, N., ASHOK, R., MANIKANDAN, S., et al. All-analog adaptive equalizer for coherent data center interconnects. *Journal of Lightwave Technology*, 2020, vol. 38, no. 21, p. 5867–5874. DOI: 10.1109/JLT.2020.2987140

[43] FATADIN, I., IVES, D., SAVORY, S. J. Blind equalization and carrier phase recovery in a 16-QAM optical coherent system. *Journal of Lightwave Technology*, 2009, vol. 27, no. 15, p. 3042–3049. DOI: 10.1109/JLT.2009.2021961

[44] CHEN, S., CHNG, E. S. Concurrent constant modulus algorithm and soft decision directed scheme for fractionally-spaced blind equalization. In *IEEE International Conference on Communications*. Paris (France), 2004, p. 2342–2346. DOI: 10.1109/ICC.2004.1312937

[45] HAYKIN, S. *Unsupervised Adaptive Filtering*. 2nd ed., rev. New York (United States): John Wiley & Sons, 2000. ISBN: 0471379417

[46] SAVORY, S. J. Digital filters for coherent optical receivers. *Optics Express*, 2008, vol. 16, no. 2, p. 804–817. DOI: 10.1364/OE.16.000804

[47] ANTONELLI, C., MECOZZI, A. Statistics of the DGD in PMD emulators. *IEEE Photonics Technology Letters*, 2004, vol. 16, no. 8, p. 1840–1842. DOI: 10.1109/LPT.2004.829771

[48] ZHU, Y., LI, A., PENG, W.-R., et al. Spectrally-efficient single-carrier 400G transmission enabled by probabilistic shaping. In *Proceedings of Optical Fiber Communications Conference and Exposition (OFC)*. Los Angeles (United States), 2017, p. 1–3. DOI: 10.1364/OFC.2017.M3C.1

[49] YUE, Y., WANG, Q., ANDERSON, J. Transmitter skew tolerance and spectral efficiency tradeoff in high baud-rate QAM optical communication systems. *Optics Express*, 2018, vol. 26, no. 12, p. 15045–15058. DOI: 10.1364/OE.26.015045

[50] PERIN, J. K., SHASTRI, A., KAHN, J. M. Design of low-power DSP-free coherent receivers for data center links. *Journal of Lightwave Technology*, 2017, vol. 35, no. 21, p. 4650–4662. DOI: 10.1109/JLT.2017.2752079

About the Authors . . .

Kayol Soares MAYER received the B.Sc. degree in Automation and Control Engineering from the Pontifical Catholic University of Rio Grande do Sul – PUCRS, in 2016, and the M.Sc. degree in Electrical Engineering, also from PUCRS, in 2018. Currently, he is a Ph.D. Candidate in Electrical Engineering at the University of Campinas – Unicamp. His current research interests include wireless and optical communications, adaptive digital signal processing, and machine learning.

Jonathan Aguiar SOARES received the B.Sc. degree in Electrical Engineering from the Pontifical Catholic University of Rio Grande do Sul – PUCRS, in 2018, and the M.Sc. degree in Electrical Engineering from the University of Campinas – Unicamp, in 2021. Currently, he is a Ph.D. Student in Electrical Engineering at Unicamp. His current research interests include wireless communications, digital signal processing, and machine learning.

Dalton Soares ARANTES received the Bachelor degree in Electronics Engineering from Federal University of Rio de Janeiro – UFRJ, where in 1968/69 he also attended several graduate courses at COOPE/UFRJ. In 1971 he joined the School of Engineering at the University of Campinas – Unicamp, where he started his academic career as an Assistant Professor and in 1972 obtained his Master degree in Electrical Engineering. In 1976 he obtained the Ph.D. degree in Electrical Engineering from the School of Electrical Engineering, Cornell University, Ithaca, New York, USA. His main areas of interest include DSP for Telecommunications, Channel Equalization, Synchronization Techniques, Coherent Optical Communications, Wireless Communications.